applied optics

Demodulation of multimodulation artifacts in Fourier-transform infrared spectroscopy

MATHIAS SCHILLING[1,2] AND JÜRGEN STOHNER[2,3,*]

[1]Current address: Metrohm AG, Ionenstrasse, CH-9100 Herisau, Switzerland
[2]Institute of Chemistry and Biotechnology (ICBT), Zurich University of Applied Sciences (ZHAW), Einsiedlerstrasse 31, CH-8820 Wädenswil, Switzerland
[3]Guest scientist at: Laboratory for Physical Chemistry, ETH Zürich, Wolfgang-Pauli-Strasse 10, CH-8093 Zürich, Switzerland
*Corresponding author: juergen.stohner@zhaw.ch

Received 21 February 2017; revised 21 March 2017; accepted 21 March 2017; posted 7 April 2017 (Doc. ID 287105); published 5 May 2017

Fourier-transform infrared (FTIR) spectra can show artifacts, for example, in the vicinity of the overtone when light is doubly modulated. Technical approaches, i.e., modifications to the spectrometer setup, have been devised in order to reduce those artifacts. Elimination of the artifacts was achieved only partly but at the expense of a loss of intensity or an increase in the noise level. We devised a computational demodulation scheme that is capable of almost fully reducing the artifacts with neither a loss of spectroscopic information nor an increase in the noise level. This has been demonstrated for the FTIR absorption spectra in the overtone regions of HCl(g) and CH_4(g).

OCIS codes: (070.4560) Data processing by optical means; (080.4035) Mirror system design; (120.5700) Reflection; (290.2745) Ghost reflections; (300.6340) Spectroscopy, infrared.

https://doi.org/10.1364/AO.56.004076

1. INTRODUCTION

Fourier-transform infrared spectroscopy (FTIR) is a universal tool for the analysis of chemical compounds due to their fingerprint characteristic absorption in the infrared spectral range. With the advent of Fourier transformation, recording of a spectrum with high to medium resolution became very fast. Since the pioneering work of Jacquinot and Fellgett [1] in the early 1950s, Michelson's interferometric absorption spectroscopy became a routine tool. With the advent of computers and the algorithmic developments of the fast Fourier transform (FFT) by Cooley and Tukey in 1965 [2], FT spectroscopy increased its applicability to spectral ranges from lower energy (microwave [3], nuclear magnetic resonance [4]) to higher energy (UV/VIS [5,6]).

Rovibrational spectra of molecules in the gas phase are recorded for an unambiguous assignment of corresponding transitions [7]. In standard routine analytical applications, medium resolution is often sufficient. Contrary to the obvious advantages of the Fourier techniques, multimodulation artifacts can arise due to backreflection of the IR beam into the interferometer; those artifacts appear at multiples of the energy associated with absorption signals in the fundamental and overtone spectral regions [8–21]. These artifacts with lower intensity at multiples of fundamentals thus overlap in part with overtones, which are anharmonically shifted toward lower energy. Artifacts due to aperture were observed in the past for CO and CO_2 in the gas phase [8,11,12]. A few technical approaches to reduce or fully eliminate these artifacts by modifying apertures such that no backreflection should occur were proposed in the past [8–10], but those modifications led to an intensity loss and/or to an increase in the noise level.

We report here artifacts for gaseous HCl between 5400 and 6200 cm^{-1} and CH_4 between 5800 and 6400 cm^{-1}, which extend over a broad spectral range and strongly overlap with overtone and combination bands, thereby perturbing the line shapes as well as intensities. It seems that those artifacts are more a characteristic feature of interferometric systems rather than a rare effect. Therefore, we devised a computational scheme to strongly reduce or even eliminate those artifacts numerically by neither loosing intensity nor increasing the noise level. In addition, we propose a device-oriented modification (use of a special mirror and setup with multiple detectors) that would, in principle, allow for a fully computerized automated compensation [19,20].

2. DESCRIPTION OF THE DEMODULATION SCHEME

A. Single Reflection at a Point in Front of the Sample Cell

First, we consider a single reflection between the mirror C2 and the sample cell F (see Fig. 1) causing the double modulation of

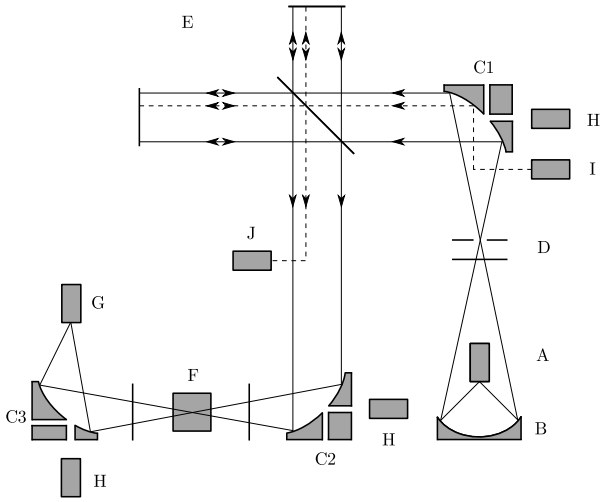

Fig. 1. Proposed modifications for a FTIR spectrometer containing a source (A), reflection optics (spherical mirror B, parabolic mirrors C1 and C2, and elliptic mirrors C3), filters and apertures (D), Michelson-type interferometer (E), sample cell (F), main detector (G), secondary detectors (H), reference laser (I), and its detector (J).

the total interference signal. The underlying idea of our compensation method for a Michelson-type interferometer uses the fact that the detected interference signal can be decomposed into parts, thereby following the directions outlined by Chamberlain [22]. Thus, the detected interference signal is a superposition of two (or more) interference signals depending on the mirror offset x, one single modulated I_s, and one double modulated I_d by the interferometer:

$$I(x) = I_s(x) + I_d(x). \tag{1}$$

In order to minimize or better fully compensate artifacts, we aim to subtract a correction interference signal, $I_{\text{corr}}(x)$, from the experimental one, $I(x)$, thereby cancelling the term of the double modulation. A compensated interference signal, $I_{\text{comp}}(x)$, is obtained as follows:

$$\begin{aligned} I_{\text{comp}}(x) &= I(x) - \gamma I_{\text{corr}}(x) \\ &= (I_s(x) + I_d(x)) - \gamma(I_s(2x) + I_d(2x)). \end{aligned} \tag{2}$$

γ denotes a compensation coefficient, in our system with $0 \le \gamma < 1$. If the double-modulated interference signal $I_d(x)$ is equal to the single-modulated interference signal at twice the mirror offset, $I_s(2x)$, times the compensation coefficient γ,

$$I_d(x) \stackrel{!}{=} \gamma I_s(2x). \tag{3}$$

$I_d(x)$ is cancelled, thereby generating a new interference signal with newly introduced but much reduced artifacts at double the mirror offset of the original artifacts, which leads to

$$I_{\text{comp}}(x) = I_s(x) - \gamma I_d(2x). \tag{4}$$

We can repeat this idea of succinct compensation by introducing higher terms in the mirror offset (e.g., 4-fold, 8-fold, 16-fold,…) resulting in

$$\underline{n = 0}$$

$$I_{\text{comp}}(x) = \frac{1}{2} I_0(\tilde{\nu})(1 + \cos(2\pi\tilde{\nu}x))\tau_A\tau_{R,s}\gamma_0 \tag{5a}$$

$$+ \frac{1}{2} I_0(\tilde{\nu})(1 + \cos(2\pi\tilde{\nu}2x))\tau_A\tau_{R,d}\gamma_0, \tag{5b}$$

$$\underline{n = 1}$$

$$- \frac{1}{2} I_0(\tilde{\nu})(1 + \cos(2\pi\tilde{\nu}2x))\tau_A\tau_{R,s}\gamma_1 \tag{5c}$$

$$- \frac{1}{2} I_0(\tilde{\nu})(1 + \cos(2\pi\tilde{\nu}4x))\tau_A\tau_{R,d}\gamma_1, \tag{5d}$$

$$\underline{n = m} \qquad \vdots$$

$$+ (-1)^m \frac{1}{2} I_0(\tilde{\nu})(1 + \cos(2\pi\tilde{\nu}2^m x))\tau_A\tau_{R,s}\gamma_n \tag{5e}$$

$$+ (-1)^m \frac{1}{2} I_0(\tilde{\nu})(1 + \cos(2\pi\tilde{\nu}2^{m+1} x))\tau_A\tau_{R,d}\gamma_n. \tag{5f}$$

$I_0(\tilde{\nu})$ denotes the incident power, which depends on the wavenumber $\tilde{\nu}$. The $\tilde{\nu}$-dependent transmissivity ascribed to pure absorptive loss is denoted as τ_A, and the $\tilde{\nu}$-dependent transmissivity ascribed to all causes other than absorption (reflection effects) is denoted as τ_R, with $0 \le \tau_A\tau_R < 1$ [22]. The compensation coefficients $\gamma_n (n = 0, 1, 2, \ldots m)$ are

$$\gamma_0 = \left(\frac{\tau_{R,d}}{\tau_{R,s}}\right)^0, \tag{6a}$$

$$\gamma_1 = \left(\frac{\tau_{R,d}}{\tau_{R,s}}\right)^1, \tag{6b}$$

$$\vdots$$

$$\gamma_m = \left(\frac{\tau_{R,d}}{\tau_{R,s}}\right)^m. \tag{6c}$$

The correction coefficient γ depends on the transmittance coefficient related to reflection, τ_R. We assume a slow change in τ_R in the wavenumber domain and therefore also a small change in the spatial domain of the interferogram. γ will then be treated as a constant that is independent of the mirror offset x. For example, applying the compensation scheme once ($n = 1$), we see that terms Eqs. (5b) and (5c) compensate exactly. The compensation interference signal $I(x)_{\text{comp}}$ contains only a single modulated contribution, Eq. (5a), and a 4-fold modulated contribution, Eq. (5d), which has much lower intensity than $I_s(x)$ and $I_d(x)$. This follows from the fact that Eq. (5a) scales as

$$\tau_{R,s}\gamma_0 = \tau_{R,s}\left(\frac{\tau_{R,d}}{\tau_{R,s}}\right)^0 = \tau_{R,s}, \tag{7}$$

whereas Eq. (5d) scales as

$$\tau_{R,d}\gamma_1 = \tau_{R,d}\left(\frac{\tau_{R,d}}{\tau_{R,s}}\right)^1. \tag{8}$$

Since $\tau_{R,s} \gg \tau_{R,d}$, the term represented in Eq. (5d) is smaller than the contributions from Eqs. (5a) and (5b). From the

discussion above for the case of $n = 1$, we see that every additional iterative compensation leads to a further decrease by a factor of $(\tau_{R,d}/\tau_{R,s})$.

Equation (5) can be written in a more compact form as

$$I(x)_{\text{comp}} = \sum_{n=0}^{m} (-1)^n \frac{1}{2} I_0(\tilde{\nu})[(1 + \cos(2\pi 2^n \tilde{\nu}x))\tau_A \tau_{R,s} + (1 + \cos(2\pi 2^{n+1}\tilde{\nu}x))\tau_A \tau_{R,d}]\gamma_n, \quad (9)$$

with

$$\gamma_n = \left(\frac{\tau_{R,d}}{\tau_{R,s}}\right)^n. \quad (10)$$

Due to alias overlap, the newly produced artifacts at $2x$, $4x$, $8x$, … or $2\tilde{\nu}$, $4\tilde{\nu}$, $8\tilde{\nu}$, …, respectively, can be folded back into the spectrum. Equation (9) can also be extended to compensate for higher order modulations by replacing 2^n and 2^{n+1} (double modulation) with k^n and k^{n+1} (k-fold modulation).

B. Two Reflections: One in Front and One behind the Sample Cell

In this subsection, we consider two reflections: one between C2 and F and one between F and G; see Fig. 1. For such a system, the interference signal $I(x)$ takes the form

$$I(x) = I_s + I_{d1} + I_{d2}. \quad (11)$$

I_s designates the single-modulated interference signal, I_{d1} describes the double-modulated interference signal between C2 and F, whereas I_{d2} is the double-modulated interference signal between F and G (Fig. 1). In the case of I_{d2}, we assume that the beam is reflected back into the interferometer once (thus double-modulated) at the left window of the sample cell before leaving toward the detector. In this case, the beam crosses the sample cell three times, which leads to τ_A^p ($p = 3$), Eq. (12c). For I_{d1}, the beam is reflected back into the interferometer at the right window of the sample cell (double-modulated) before leaving the sample cell toward the detector. In this case, the beam passes the sample cell once. Therefore, τ_A ($p = 1$), Eq. (12b). There is no fundamental reason why $\tau_{R,d1}$ and $\tau_{R,d2}$ should be equal. Therefore, we retain them as separate parameters,

$$I(x) = \frac{1}{2} I_0(\tilde{\nu})[(1 + \cos(2\pi\tilde{\nu}x))\tau_A \tau_{R,s} \quad (12a)$$

$$+(1 + \cos(2\pi\tilde{\nu}2x))\tau_A \tau_{R,d1} \quad (12b)$$

$$+(1 + \cos(2\pi\tilde{\nu}2x))\tau_A^p \tau_{R,d2}]. \quad (12c)$$

Analogous to Section 2.1, Eq. (1), the terms I_{d1} and I_{d2} in Eq. (12c) have to be eliminated. A compensated interference signal, $I_{\text{comp}}(x)$, is therefore obtained as follows:

$$\begin{aligned} I_{\text{comp}}(x) &= I(x) - \gamma I_{\text{corr}}(x) \\ &= (I_s(x) + I_{d1}(x) + I_{d2}(x)) \\ &\quad -\gamma(I_s(2x) + I_{d1}(2x) + I_{d2}(2x)), \end{aligned} \quad (13)$$

with

$$I_{d1}(x) + I_{d2}(x) \stackrel{!}{=} \gamma I_s(2x). \quad (14)$$

The general compensation coefficient γ_n for n compensations is, in this case, found to be

$$\gamma_n = \left(\frac{\tau_A \tau_{R,d1} + \tau_A^p \tau_{R,d2}}{\tau_A \tau_{R,s}}\right)^n. \quad (15)$$

Similar to Eq. (5), the first iteration of the compensation scheme yields

$$\underline{n = 0}$$

$$I(x)_{\text{comp}} = \frac{1}{2} I_0(\tilde{\nu})(1 + \cos(2\pi\tilde{\nu}x))\tau_A \tau_{R,s}\gamma_0, \quad (16a)$$

$$+\frac{1}{2} I_0(\tilde{\nu})(1 + \cos(2\pi\tilde{\nu}2x))\tau_A \tau_{R,d1}\gamma_0, \quad (16b)$$

$$+\frac{1}{2} I_0(\tilde{\nu})(1 + \cos(2\pi\tilde{\nu}2x))\tau_A^p \tau_{R,d2}\gamma_0, \quad (16c)$$

$$\underline{n = 1}$$

$$-\frac{1}{2} I_0(\tilde{\nu})(1 + \cos(2\pi\tilde{\nu}2x))\tau_A \tau_{R,s}\gamma_1, \quad (16d)$$

$$-\frac{1}{2} I_0(\tilde{\nu})(1 + \cos(2\pi\tilde{\nu}4x))\tau_A \tau_{R,d1}\gamma_1, \quad (16e)$$

$$-\frac{1}{2} I_0(\tilde{\nu})(1 + \cos(2\pi\tilde{\nu}4x))\tau_A^p \tau_{R,d2}\gamma_1, \quad (16f)$$

$$=\frac{1}{2} I_0(\tilde{\nu})(1 + \cos(2\pi\tilde{\nu}x))\tau_A \tau_{R,s}, \quad (16g)$$

$$-\frac{1}{2} I_0(\tilde{\nu})(1 + \cos(2\pi\tilde{\nu}4x))\tau_A \frac{\tau_{R,d1}^2}{\tau_{R,s}}, \quad (16h)$$

$$-2 \cdot \frac{1}{2} I_0(\tilde{\nu})(1 + \cos(2\pi\tilde{\nu}4x))\tau_A^p \frac{\tau_{R,d1}\tau_{R,d2}}{\tau_{R,s}}, \quad (16i)$$

$$-\frac{1}{2} I_0(\tilde{\nu})(1 + \cos(2\pi\tilde{\nu}4x))\tau_A^{2p-1} \frac{\tau_{R,d2}^2}{\tau_{R,s}}. \quad (16j)$$

If we apply our correction scheme once, i.e., $n = 1$, the terms in Eqs. (16b) and (16c) are compensated by Eq. (16d). This can be seen by observing that from Eqs. (16b) and (16c),

$$\tau_A \tau_{R,d1}\gamma_0 = \tau_A \tau_{R,d1}, \quad (17)$$

and

$$\tau_A^p \tau_{R,d2}\gamma_0 = \tau_A^p \tau_{R,d2}. \quad (18)$$

We obtain

$$\tau_A \tau_{R,s}\gamma_1 = \tau_A \tau_{R,s} \frac{\tau_A \tau_{R,d1} + \tau_A^p \tau_{R,d2}}{\tau_A \tau_{R,s}} = \tau_A \tau_{R,d1} + \tau_A^p \tau_{R,d2}. \quad (19)$$

Equations (16e) and (16f) are replaced by the contributions in Eqs. (16h)–(16j).

The compensation interference signal $I_{\text{comp}}(x)$ contains only a single modulated contribution [Eq. (16g)] and 4-fold modulated contributions, Eqs. (16h)–(16j), with lower intensities than I_s, I_{d1}, and I_{d2}; this follows from similar reasoning as described in Section 2.1.

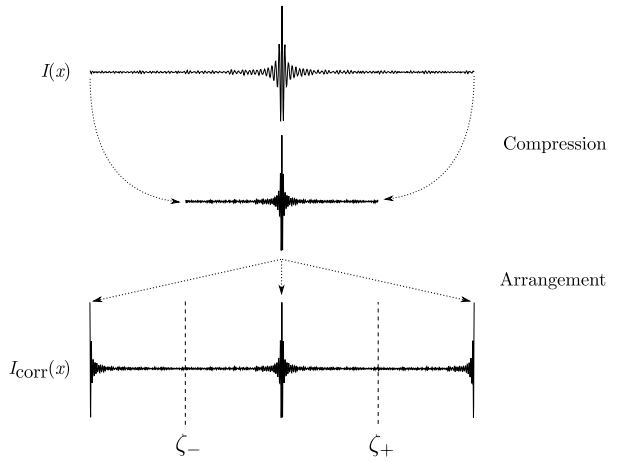

Fig. 2. Method for generating I_{corr} for compensation used in Eq. (2).

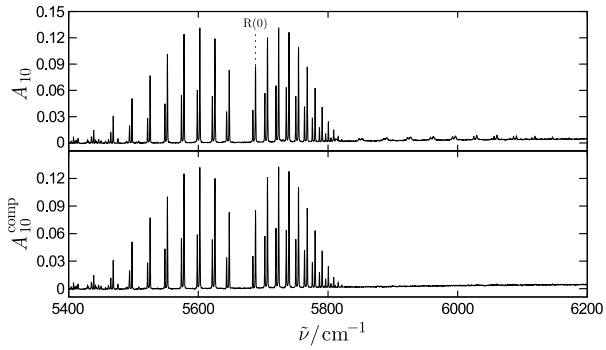

Fig. 3. First overtone of HCl (5400 to 5830 cm^{-1}, resolution 0.5 cm^{-1}) with the double-modulation artifacts associated with the fundamental of HCl. The original spectrum (upper trace) was compensated (lower trace) with a single iteration using Eq. (2) and $\gamma_1 = 0.004$. The correction interferogram I_{corr} was arranged as shown in Fig. 2.

3. PRACTICAL IMPLEMENTATION

The main aspect of the practical implementation of Eq. (2) is to determine the correction interference function $I_{\mathrm{corr}}(x)$ by doubling the frequency. One possibility to achieve this is to remove every second data point of the original interference function $I(x)$. The compressed interference function $I(2x) = I_{\mathrm{corr}}(x)$ is also centered around the point of zero path difference, see Fig. 2, which illustrates the compensation procedure for a double-sided single-directional interferogram.

In principle, one can distinguish two ways to obtain the correction interference function $I_{\mathrm{corr}}(x)$. First, one would construct $I_{\mathrm{corr}}(x)$ by increasing the resolution: recording an interferogram of 2^n-fold increased length more than needed in the end (corresponds to 2^n-fold resolution) and one uses only 1/2 of the interferogram for each repetition of the demodulation scheme. This guarantees that the final compensated interferogram has the same resolution as the originally recorded interferogram. Here, we explore a second scheme, depicted in Fig. 2. In a first step, we compress the interferogram to half its length by deleting every second data point. The result is an interferogram of half the original length (from ζ_+ to ζ_-, Fig. 2). The points marked ζ_+ and ζ_- are used to mirror the compressed interferogram, thereby constructing $I_{\mathrm{corr}}(x)$ of original length, i.e., without loss of resolution, in contrast to the first method described above. Many more possibilities to obtain $I_{\mathrm{corr}}(x)$ can be envisaged; this has been explored in great detail [19].

4. RESULTS AND DISCUSSION

In this section, we present two examples of gas-phase spectra showing the double-modulation artifacts, namely, HCl(g) and CH_4(g) in their respective overtone regions [19,20]. First, the correction scheme described in Fig. 2 is applied to the spectrum of HCl(g).

A. Hydrogen Chloride Gas

We present the corrected spectrum for HCl(g) (lower trace) together with the original spectrum (upper trace) recorded between 5400 and 6200 cm^{-1} in Fig. 3.

The corrected spectrum has been obtained considering double modulation with a constant compensation coefficient $\gamma_1 = 4 \cdot 10^{-3}$. One can see immediately that the artifacts associated with the fundamental band are strongly compensated by our correction scheme, which has been applied once [$n = 1$, Eq. (5)]. Spectral information of the fundamental (line positions and line intensities) and the overall noise level do not change appreciably upon correction.

For illustrative purposes, we discuss the influence of our correction scheme on the absorption in more detail and therefore calculated the interferograms of the fundamental and the first overtone of the rovibrational spectrum of HCl(g) with and without double modulation. We select HCl(g) because of the simplicity of the absorption spectrum in comparison with CH_4(g) and the accessibility of the respective spectroscopic parameters (after [23,24]): we have compared our measured spectrum before and after correction with a simulated spectrum of HCl(g) where spectroscopic parameters have been taken from HITRAN [24] and found good agreement. It is to be expected that absorbances are more sensitive to corrections than are line positions; our analysis has shown that the absorbance changes due to our correlation scheme are very small. We have to simulate two interferograms twice, namely, an interferogram of the background (empty sample cell) and an interferogram of the sample for single and double modulation. In the latter case, we choose the parameters such that the simulated spectrum resembles the measured spectrum shown in Fig. 3. Our simulation without double modulation uses $\tau_{R,s} = 1$ and $\tau_{R,d} = 0$. The simulation with double modulation uses $\tau_{R,s} = 0.996$ and $\tau_{R,d} = 0.004$. Figure 4 shows the simulated spectrum of HCl(g) with the compensation parameters just described. The upper trace, Fig. 4(a), displays the simulated spectrum without double modulation, the middle trace, Fig. 4(b), shows the spectrum with double modulation and the lower trace, Fig. 4(c), shows the compensated spectrum with single demodulation [$n = 1, \gamma_1 = \tau_{R,d}/\tau_{R,s} = 0.004/0.996$; see Eq. (6b)]. With these simulations, we can quantify the change of absorbance upon considering the double modulation. We can also quantify the effect of our compensation scheme with respect to the

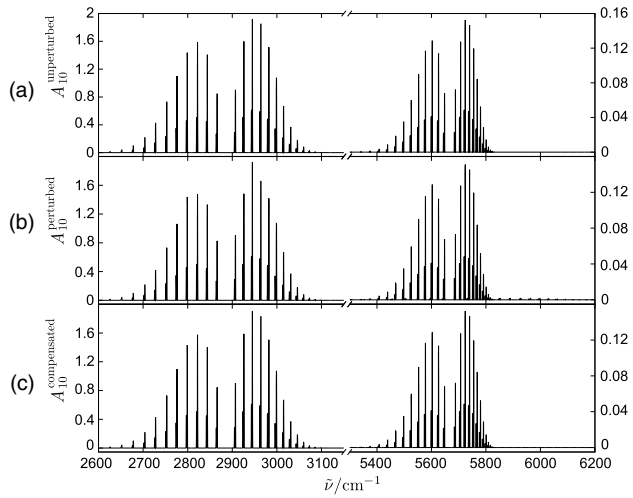

Fig. 4. Simulated spectra of HCl(g). (a) $A_{10}^{\text{unperturbed}}$ obtained with $\tau_{R,s} = 1$ and $\tau_{R,d} = 0$ that is without double modulation (after [23,24]). The spectra were adjusted such as to match the absorbance values of the experiment for better comparability. (b) $A_{10}^{\text{perturbed}}$ obtained with $\tau_{R,s} = 0.996$ and $\tau_{R,d} = 0.004$, which introduces the artifacts caused by double modulation visible above 5800 cm^{-1}. (c) $A_{10}^{\text{compensated}}$ obtained from $\tau_{R,s} = 0.996$ and $\tau_{R,d} = 0.004$ with the compensation parameter $\gamma_1 = 0.004/0.996$. This demodulation eliminates the artifacts above 5800 cm^{-1} completely.

original spectrum with and without double modulation. Numbers for these comparisons are given in Table 1 for the fundamental and in Table 2 for the first overtone of HCl(g). In order to quantify the effect of our compensation scheme on line intensities represented by A_{10}, we need to calculate an interferogram with and without double modulation because measured interferograms always contain contributions from double or even multiple modulations. We used wavenumber-independent $\tau_{R,d} = 0.004$ and $\tau_{R,s} = 0.996$, which signify that no light intensity is lost, where $\tau_{R,d}$ is assumed to be about equal to the natural reflection coefficient of KBr-window material of our gas cell. The compensation coefficient γ_m depends on $\tau_{R,s}$ and $\tau_{R,d}$, Eq. (6b).

Table 1 shows the selected R-branch [$R(J'')$, $J'' = 1, 2, \ldots 6$]. For the R-branch we have $\Delta J = J' - J'' = +1$, where the upper and lower J-states of the rotational transition are indicated by prime $'$ and double prime $''$ symbols. The corresponding R-branch absorbance A_{10} of the spectrum without double modulation (unperturbed) of the double-modulated spectrum obtained with parameters as described above as well as the absorbance after compensation (demodulated) are shown in columns 2 to 6. If one compares the double-modulated absorbance with the unperturbed ones, we see that the relative change $\Delta A_{10}^{\text{sim}}$ (column 4) decreases by values between -10^{-4}% and about −10%. No systematic trend can be observed depending on J. After compensation (demodulation), the absorbance changes $\Delta A_{10}^{\text{sim}}/\%$ (column 6) are obtained from the deviation of the ratio A_{10} (demodulated) to A_{10} (unperturbed) with respect to 1:

$$\Delta A_{10}^{\text{sim}} = 1 - \frac{A_{10}}{A_{10}(\text{unperturbed})}, \tag{20}$$

where A_{10} on the right-hand side of Eq. (20) stands for the demodulated or the double-modulated absorbance. It seems that the deviation caused by introducing double modulation (columns 3 and 4) is for some transitions compensated by our scheme, which then results in smaller relative deviations after compensation (columns 5 and 6).

Similar observations hold for the first overtone of HCl(g) and the corresponding numbers are given in Table 2. They refer to the absorbance for the case without double modulation (unperturbed), with double modulation (columns 3 and 4),

Table 1. Selected *R*-Branch Lines of the Fundamental of HCl(g) for Analysis[a]

	Unperturbed	Double Modulation		Compensated	
Transition	A_{10}	A_{10}	$\Delta A_{10}^{\text{sim}}/\%$	A_{10}	$\Delta A_{10}^{\text{sim}}/\%$
$R(2)$	1.922056	1.922042	−0.000740	1.922056	0.000034
$R(3)$	1.856042	1.661998	−10.454721	1.851059	−0.268434
$R(4)$	1.517049	1.418848	−6.473162	1.517169	0.007968
$R(5)$	1.076376	1.076374	−0.000222	1.076376	0.000017
$R(6)$	0.670813	0.670813	−0.000037	0.670388	−0.063372

[a]The percentage difference between no modulation (unperturbed), double modulation, and compensation (demodulated) is reported as $\Delta A_{10}^{\text{sim}}$. The double-modulated interferogram was calculated with $\tau_{R,s} = 0.996$ and $\tau_{R,d} = 0.004$. Therefore, $\gamma_1 = 0.004/0.996$; see Eq. (6b).

Table 2. Selected *R*-Branch Lines of the First Overtone of HCl(g) for Analysis[a]

	Unperturbed	Double Modulation		Compensated	
Transition	A_{10}	A_{10}	$\Delta A_{10}^{\text{sim}}/\%$	A_{10}	$\Delta A_{10}^{\text{sim}}/\%$
$R(2)$	0.152627	0.151174	−0.951683	0.152601	−0.016641
$R(3)$	0.146778	0.145391	−0.944965	0.146781	0.002383
$R(4)$	0.119580	0.119580	−0.000071	0.119578	−0.001984
$R(5)$	0.084522	0.083780	−0.877499	0.084510	−0.013566
$R(6)$	0.052485	0.052041	−0.845184	0.052489	0.007801

[a]The percentage difference between no modulation (unperturbed), double modulation, and compensation (demodulated) is reported as $\Delta A_{10}^{\text{sim}}$. The double-modulated interferogram was calculated with $\tau_{R,s} = 0.996$ and $\tau_{R,d} = 0.004$. Therefore, $\gamma_1 = 0.004/0.996$; see Eq. (6b).

and after compensation ($n = 1$, columns 5 and 6). We used the same values for $\tau_{R,s}$, $\tau_{R,d}$, and γ_1 as for the fundamental of HCl (g). The double-modulated absorbances show relative changes ($\Delta A_{10}^{\mathrm{sim}}$, column 4) between $7 \cdot 10^{-5}$% and –1.0% without systematic changes with respect to J. The values for the changes in absorbances $\Delta A_{10}^{\mathrm{sim}}$ after demodulation have been obtained as described above and are comparable in magnitude to those values obtained for the fundamental absorption of HCl(g). Again, we observe that the artifacts can be compensated completely without affecting the noise-level appreciably.

The question arises whether or not the change in absorbance upon comparing simulations without demodulation (unperturbed), with double modulation, and with demodulation depend on the value of γ_1. If one uses a value of γ_1 that is too large, one overcompensates the artifacts, which leads to unphysical negative absorbances in the spectral regions of the artifacts. Figure 5 shows $\Delta A_{10}^{\mathrm{exp}}$ of HCl(g) for individual transitions of the fundamental band [Fig. 5(a)], the first overtone [Fig. 5(b)], and the artifacts [Fig. 5(c)]. The values have been obtained according to

$$\Delta A_{10}^{\mathrm{exp}} = \frac{A_{10}^{\mathrm{comp}}}{A_{10}^{\mathrm{exp}}} - 1 \qquad (21)$$

from the compensated A_{10}^{comp} (demodulated or compensated, comp) and the experimental A_{10}^{exp} (experimental, exp) values. To obtain those numbers, we scanned the value of γ_1 between 0 and 0.01 in steps of 0.001, which results in γ_1-dependent values of A_{10}^{comp}. The corresponding experimental absorbances of the overtone and the artifacts are shown in Fig. 3 (upper trace).

For a particular value of γ_1, we determined $\Delta A_{10}^{\mathrm{exp}}$ in the depicted spectral regions of the fundamental [Fig. 5(a)], the first overtone [Fig. 5(b)], and in the region where the artifacts appear [Fig. 5(c)] for $R(2)$ to $R(6)$. In case of the fundamental region [Fig. 5(a)], $\Delta A_{10}^{\mathrm{exp}}$ varies with γ_1; some transitions show strong dependence [e.g., $R(3)$], whereas others seem to be largely independent of γ_1 [e.g., $R(6)$]. Maximum $\Delta A_{10}^{\mathrm{exp}}$ values are of the order of 5% for the interval depicted here. In Fig. 5(b), the $\Delta A_{10}^{\mathrm{exp}}$ values of the overtone change with γ_1 with no strong dependence on the particular transition.

The aim of our compensation scheme is to minimize the signals of the artifacts. In the ideal case and in the absence of noise, we would seek to achieve a $\Delta A_{10}^{\mathrm{exp}}$ value of –100%, which would compensate the artifact exactly. As can be seen from Fig. 5(c), this compensation can be achieved in the range of $0.0037 < \gamma_1 < 0.0050$ (vertical dotted lines), however, this condition cannot be fulfilled strictly for all artifacts at the same time. The shaded box marks the region between about one standard deviation of the noise level (roughly ±10%). Outside the region of the vertical dotted lines, over- or under-compensation would take place. The interval for γ_1 can be chosen according to an acceptable tolerance level for the compensation.

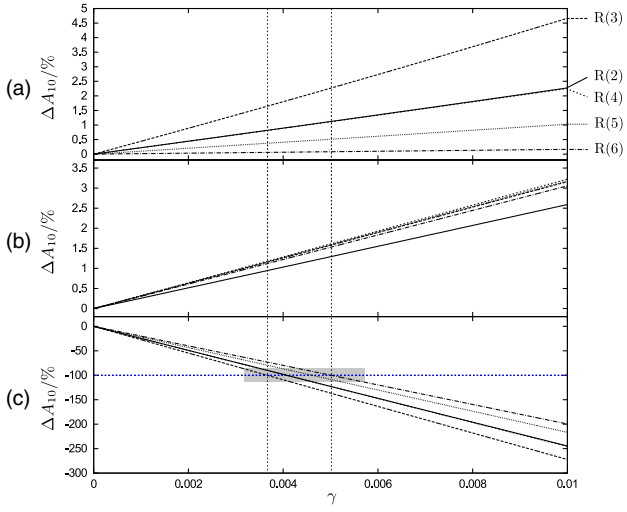

Fig. 5. Percentage change of selected rotational lines of HCl [$R(2)$ to $R(6)$] when applying the compensation scheme with the compensation coefficient γ between 0 and 0.01. The change of the fundamentals is shown in (a) and the first overtone in (b). The respective artifacts are shown in (c). The horizontal line at –100% indicates the values of γ, at which the selected artifacts are compensated completely.

B. Methane Gas

The correction scheme described in Fig. 2 is now applied to the spectrum of CH_4(g). Figure 6 shows the original spectrum (upper trace) of the P_4-tetradecad band of methane between 5800 and 6150 cm^{-1} [25,26], centered around 6000 cm^{-1}, and its corrected form (lower trace). The corrected spectrum has been obtained considering double modulation with a constant compensation coefficient $\gamma = 4 \cdot 10^{-3}$. One can see immediately that the artifacts associated with the P_2-pentad band centered around 3000 cm^{-1} are strongly compensated by our correction scheme, which has been applied once [$n = 1$, Eq. (5)]. Spectral information of the P_4-tetradecad and the overall noise level do not change appreciably upon correction. The broad absorption feature underlying the $R(0)$ to $R(2)$ transition (about 6000 to 6050 cm^{-1}) is due to the Q-branch artifact of the P_2-pentad. After compensation, this feature is also removed with all other artifacts resulting from double modulation. Figure 7 shows $\Delta A_{10}^{\mathrm{exp}}$ of CH_4(g) for individual transitions of the P_2-pentad [Fig. 7(a)], the P_4-tetradecad [Fig. 7(b)], and the artifacts [Fig. 7(c)]. The corresponding experimental

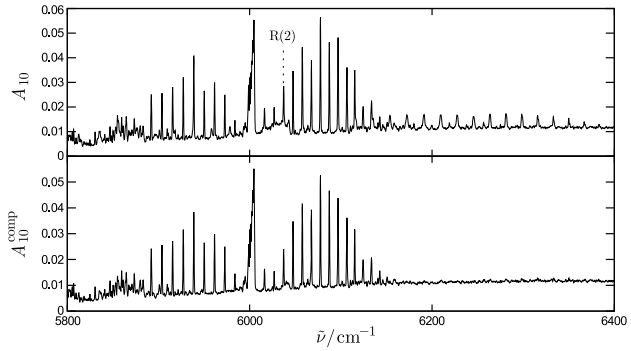

Fig. 6. P_4-tetradecad band of CH_4 (5800 to 6150 cm^{-1}, resolution 0.5 cm^{-1}) and double-modulation artifacts of the P_2-pentad band. The original spectrum (upper trace) was compensated (lower trace) with a single iteration using Eq. (2) and $\gamma = 0.004$. The correction interference function I_{corr} was arranged as shown in Fig. 2. The spectroscopic data and the assignment of the CH_4 bands were taken from Niederer [25] and Ulenikov *et al.* [26]. $R(2)$ marks a rotational line in the R-branch of the respective absorption band.

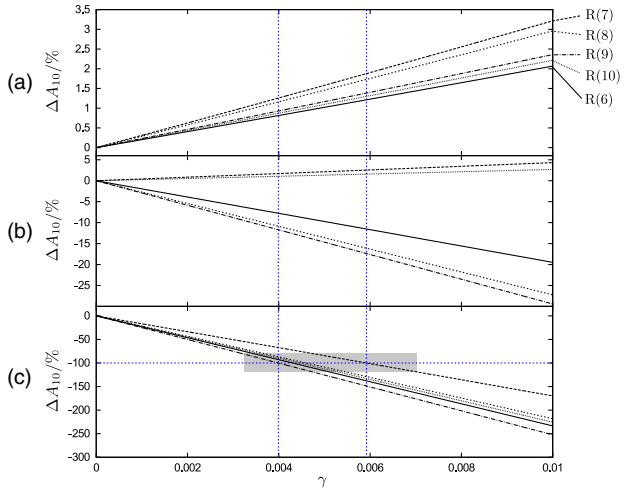

Fig. 7. Percentage change of the absorbance for selected rotational lines of CH_4 when applying the demodulation scheme with the compensation coefficient γ_1 between 0 and 0.01. The change of the selected P_2-pentad bands is shown in (a) and the change of the absorbances of the P_4-tetradecad band in (b). The respective artifacts from the P_2-pentad can be seen in (c). The horizontal line at −100% indicates the values of γ_1, at which the selected artifacts are compensated completely.

absorbances of the P_4-tetradecad and the artifacts are shown in Fig. 6 (upper trace). $\Delta A_{10}^{\mathrm{exp}}$ values have been obtained according to Eq. (21). For a particular value of γ_1, we determined $\Delta A_{10}^{\mathrm{exp}}$ in the spectral regions of the P_2-pentad [Fig. 7(a)], the P_4-tetradecad [Fig. 7(b)], and in the region where the artifacts appear [Fig. 7(c)] for $R(6)$ to $R(10)$. In the case of the P_2-pentad region [Fig. 7(a)], $\Delta A_{10}^{\mathrm{exp}}$ varies with γ_1; some transitions show stronger dependence [e.g., $R(7)$]. Maximum $\Delta A_{10}^{\mathrm{exp}}$ values are of the order of 3.5% for the interval shown here. In Fig. 7(b), the $\Delta A_{10}^{\mathrm{exp}}$ values of the P_4-tetradecad change with γ_1 with no strong dependence on the particular transition. Again, the aim of our compensation scheme is to minimize the signals of the artifacts. In the ideal case and in the absence of noise, we would seek to achieve a $\Delta A_{10}^{\mathrm{exp}}$ value of −100%, see Eq. (21), which would compensate the artifact exactly. As can be seen from Fig. 7(c), this compensation can be achieved in the range of $0.004 < \gamma_1 < 0.006$ (see vertical lines in Fig. 7), however, this condition can also not strictly be fulfilled for all artifacts at the same time, as discussed in the case of HCl(g). As can be seen from Figs. 7(b) and 7(c), larger values of γ_1 would lead to considerable overcompensation.

Up to now, we discussed compensation of interference signals in a Michelson-type interferometer, which were double-modulated. Artifacts caused by double modulation can be visualized in the spectra using the mathematical compensation scheme described above. We performed the compensation by processing the interferograms with single demodulation (using γ_m, $m = 1$) to obtain the compensated absorbance spectrum (A_{10}^{comp}). The compensation coefficient γ_1 should be chosen such that overcompensation can be avoided [see, for example, Figs. 5(c) and 7(c)]. Using the original (experimental) and compensated absorbance spectra, a difference spectrum can be calculated according to $\Delta A_{10}^{\mathrm{diff}} = A_{10}^{\mathrm{comp}} - A_{10}^{\mathrm{exp}}$ (see Fig. 8).

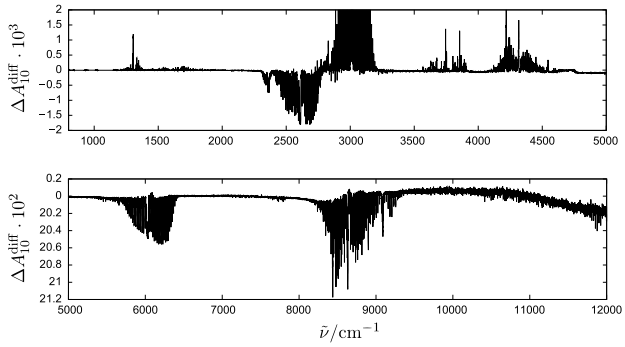

Fig. 8. Difference spectrum $\Delta A_{10}^{\mathrm{diff}} = A_{10}^{\mathrm{comp}} - A_{10}^{\mathrm{exp}}$ [Fig. 6, lower trace minus upper trace] from 800 to 12,000 cm^{-1} of CH_4 (resolution 0.5 cm^{-1}). Negative bands are compensations of the artifacts, positive signals lead of a signal raise of "true" signals. The following artifacts were found: P_1-dyad artifact at 2550 cm^{-1}, P_2-pentad artifact at 6000 cm^{-1}, P_3-octad artifact at 8600 cm^{-1}, and the P_4-tetradecad artifact at 11,750 cm^{-1}. The spectral data and the assignment of the CH_4 bands were taken from Niederer [25] and Ulenikov *et al.* [26].

In this difference spectrum, negative signals indicate artifacts in the corresponding spectral ranges. Positive signals indicate the "true" transitions, which are not artifacts caused by double modulation. Comparing the spectra A_{10}^{exp} with the difference spectrum, such artifacts can be identified easily. As shown above, a proper choice of γ_1 allows for a complete reduction of the artifacts.

For HCl and CH_4, as discussed above, a single iteration of the compensation scheme ($n = 1$) was sufficient because our artifacts were compensated to an acceptable degree caused by the smallness of $(\tau_{R,d}/\tau_{R,s})^1 = \gamma_1 \approx 4 \cdot 10^{-3}$. n counts the number of compensations and a convenient n is chosen by inspection until the introduced higher order artifacts are sufficiently compensated. Every iteration of the compensation scheme introduces higher order artifacts, which are systematically lower in intensity. Depending on the magnitude of γ_1 relative to the noise level, more than one iteration step might be necessary for an acceptable degree of compensation until the magnitude of higher order artifacts introduced is lower than the noise level.

So far, we considered artifacts caused only by double modulation. However, it would be possible to test the experimental spectra also for k-fold modulation by considering only every kth data point to generate I_{corr}; see Section 3. One would generate a compensated absorbance spectrum with, for example, $k = 4$, with the respective change in Eq. (9). A graphical representation of the difference spectrum with respect to the experiment would show negative signals for the artifacts caused by the k-fold modulation.

As an outlook, we mention briefly some ideas about an automatic procedure that might be used to determine the compensation coefficient γ by experiment. It has been demonstrated above that the key parameter for compensating artifacts caused by double modulation is γ_n, see Eq. (10), which has been determined by an iterative numerical procedure so far. As we will show here, γ_n can be determined, in principle, experimentally. By measuring a reflection interferogram, the

coefficient γ_1 can be calculated using the ratio of the intensity of the main interferogram and the intensity of the reflection interferogram. Such a reflection interferogram could be measured by introducing mirrors designed with open channels parallel to the focused beam (see Fig. 1 for C2 and C3 horizontal channels and for C1 and C3 vertical channels) and parallel to the collimated beam (see Fig. 1 for the C2 vertical channel and for the C1 horizontal channel). Placing a secondary detector H in the vicinity of one of the mirrors C1 to C3, where the reflected intensity seems to be highest, allows us to measure reflection interferograms.

Such mirrors with two channels that meet at the surface of the mirror, see Fig. 9, were used in laser spectroscopy. The main and the reflection interferogram can be detected simultaneously. For simplicity, we assume that (1) the reflection arises after passing the sample cell and (2) the detected reflection interferogram I_{refl} does not contain a contribution from double modulation (since $\tau_{R,d} \gg \tau_{R,d}^2$). The two detected interferograms (using two detectors) take the form

$$I(x) = \frac{1}{2} I_0(\tilde{\nu})[(1 + \cos(2\pi\tilde{\nu}x))\tau_A \tau_{R,s} + (1 + \cos(2\pi\tilde{\nu}2x))\tau_A^p \tau_{R,d}], \tag{22}$$

$$I_{\text{refl}}(x) = \frac{1}{2} I_0(\tilde{\nu})(1 + \cos(2\pi\tilde{\nu}x))\tau_A \tau_{R,d}, \tag{23}$$

where p is the number of times the reflected light passes the sample medium. Using $\tau_{R,s} \gg \tau_{R,d}$ as described in the previous section, the ratio I_{refl}/I can be simplified to

$$\frac{I_{\text{refl}}(x)}{I(x)} \approx \frac{\tau_{R,d}}{\tau_{R,s}} = \gamma(x). \tag{24}$$

When measuring the reflection interference signal where light is reflected in front of the gas cell, one can show that

$$\frac{I_{\text{refl}}(x)}{I(x)} \approx \frac{\tau_{R,d}}{\tau_A \tau_{R,s}} = \frac{1}{\tau_A}\gamma(x), \tag{25}$$

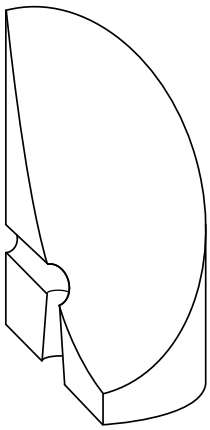

Fig. 9. Cross section of a parabolic mirror (C1 or C2) having two conic holes, see Fig. 1, one parallel to the focused beam and one parallel to the collimated beam. This is used to measure the reflection interference signal and prevent further reflections toward the interferometer [19,20].

thus yielding two slightly different expressions for γ. In the first case, where the reflection is after the sample cell, γ can be determined from the ratio of $I_{\text{refl}}(x)$ to $I(x)$ [see Eq. (24)], whereas the second case with reflection in front of the sample cell, γ is given by the ratio of $I_{\text{refl}}(x)$ to $I(x)$ weighted by the coefficient τ_A [see Eq. (25)]. However, the intensity of the detected reflection interference signal must be corrected by the illuminated areas (by the reflected light) of the mirrors placed in front of the secondary detectors and the diameter of the holes, respectively, and by the gain of the secondary detectors in relation to the main detector. This would offer a complete automation of this compensation method.

Funding. Zurich University of Applied Sciences (ZHAW) (ASF-2014/1).

Acknowledgment. We are grateful to Dr. Hans Hollenstein, ETH Zürich, for help and discussions. We thank also Dr. Li Chen and Prof. Alec M. Wodtke, University of Göttingen, for providing us with FTIR spectroscopic data on $^{13}C^{18}O$ to test our compensation scheme. JS wants to thank his academic teacher, Prof. Martin Quack (ETH Zürich), for continuous support.

REFERENCES

1. L. Mertz, "Fourier spectroscopy, past, present, and future," Appl. Opt. **10**, 386–389 (1971).
2. J. W. Cooley and J. W. Tukey, "An algorithm for the machine calculation of complex Fourier series," Math. Comput. **19**, 297–301 (1965).
3. D. W. Pratt, "Electronic spectroscopy in the gas phase," in *Handbook of High-resolution Spectroscopy*, M. Quack and F. Merkt, eds. (Wiley, 2011), Vol. **2**, pp. 1291–1320.
4. R. R. Ernst, *Nuclear Magnetic Resonance Fourier Transform Spectroscopy*, Nobel Lectures, Chemistry 1991–1995 (World Scientific, 1997), pp. 1–46.
5. T. Hirschfeld, "Fellgett's advantage in UV–VIS multiplex spectroscopy," Appl. Spectrosc. **30**, 68–69 (1976).
6. S. T. Shipman and B. H. Pate, "New techniques in microwave spectroscopy," in *Handbook of High-resolution Spectroscopy*, M. Quack and F. Merkt, eds. (Wiley, 2011), Vol. **2**, pp. 801–828.
7. F. Bauder, "Fundamentals of rotational spectroscopy," in *Handbook of High-resolution Spectroscopy*, M. Quack and F. Merkt, eds. (Wiley, 2011), Vol. **1**, pp. 57–116.
8. T. J. Johnson, R. L. Sams, T. A. Blake, S. W. Sharpe, and P. M. Chu, "Removing aperture-induced artifacts from Fourier transform infrared intensity values," Appl. Opt. **41**, 2831–2839 (2002).
9. L. Lin, "Stray radiation estimation and interreflection correction for infrared transmittance measurement," Proc. SPIE **1331**, 179–185 (1990).
10. Bruker Optics, "Accurate reflectance and transmittance measurements on highly reflective materials," Application Note AN#12 (2009).
11. J. R. Birch and F. J. J. Clarke, "Fifty categories of ordinate error in Fourier transform spectroscopy," Spectrosc. Eur. **7**, 16–22 (1995).
12. J. R. Birch and F. J. J. Clarke, "Interreflection errors in Fourier transform spectroscopy: a preliminary appraisal," Anal. Chim. Acta **380**, 369–378 (1999).
13. D. B. Betts, F. J. J. Clarke, L. J. Cox, and J. A. Larkin, "Infrared reflection properties of five types of black coating for radiometric detectors," J. Phys. E **18**, 689–696 (1985).
14. P. R. Griffiths and J. A. de Haseth, *Fourier Transform Infrared Spectrometry* (Wiley, 2007).
15. G. Guelachvili, "Distortions in Fourier spectra and diagnosis," in *Spectrometric Techniques*, G. A. Vanasse, ed. (Academic, 1981), Vol. **II**.

16. R. C. M. Learner, A. P. Thorne, and J. W. Brault, "Ghosts and artifacts in Fourier-transform spectrometry," Appl. Opt. **35**, 2947–2954 (1996).
17. B. Saggin, L. Comolli, and V. Formisano, "Mechanical disturbances in Fourier spectrometers," Appl. Opt. **46**, 5248–5256 (2007).
18. M. Schilling, "Identifikation und Behebung von Geistersignalen im FT-IR Schwingungsrotationsspektrum von HCl," B.Sc. thesis (Zurich University of Applied Sciences (ZHAW), 2013) (unpublished).
19. M. Schilling, "Device-oriented prevention and mathematical compensation of multi-modulation artefacts in Fourier transform infrared spectroscopy," M.Sc. thesis (Zurich University of Applied Sciences (ZHAW), 2016) (unpublished).
20. M. Schilling and J. Stohner, "Mathematical compensation of multi-modulation artefacts in medium resolution gas-phase spectra using Fourier transform infrared spectroscopy," in *20th Symposium on Atomic, Cluster and Surface Physics, Contributions*, J. Stohner and C. Yeretzian, eds. (Innsbruck University Press, 2016).
21. J. M. Chalmers, *Mid-Infrared Spectroscopy: Anomalies, Artifacts and Common Errors* (Wiley, 2002), pp. 2327–2347.
22. J. Chamberlain, *The Principles of Interferometric Spectroscopy* (Wiley, 1979).
23. D. U. Webb and K. N. Rao, "Vibration rotation bands of heated hydrogen halides," J. Mol. Spectrosc. **28**, 121–124 (1968).
24. L. Rothman, I. Gordon, A. Barbe, D. Benner, P. Bernath, M. Birk, V. Boudon, L. Brown, A. Campargue, J.-P. Champion, K. Chance, L. Coudert, V. Dana, V. Devi, S. Fally, J.-M. Flaud, R. Gamache, A. Goldman, D. Jacquemart, I. Kleiner, N. Lacome, W. Lafferty, J.-Y. Mandin, S. Massie, S. Mikhailenko, C. Miller, N. Moazzen-Ahmadi, O. Naumenko, A. Nikitin, J. Orphal, V. Perevalov, A. Perrin, A. Predoi-Cross, C. Rinsland, M. Rotger, M. Šimečková, M. Smith, K. Sung, S. Tashkun, J. Tennyson, R. Toth, A. Vandaele, and J. V. Auwera, "The HITRAN 2008 molecular spectroscopic database," J. Quant. Spectrosc. Radiat. Transfer **110**, 533–572 (2009).
25. J. M. G. Niederer, "The infrared spectrum of methane," Ph.D. thesis ETH Zürich Nr. 19829 (Verlag Dr. Hut, 2012).
26. O. N. Ulenikov, E. S. Bekhtereva, S. Albert, S. Bauerecker, H. M. Niederer, and M. Quack, "Survey of the high resolution infrared spectrum of methane ($^{12}CH_4$ and $^{13}CH_4$): partial vibrational assignment extended towards 12,000 cm^{-1}," J. Chem. Phys. **141**, 234302 (2014).